Light Scattering from the Spherical-Shell Atmosphere: Earth Curvature Effects Measured by SeaWiFS

PAGES 529, 530, 534

It is commonly known that the Earth's atmosphere is a spherical-shell atmosphere (SSA) rather than a plane-parallel atmosphere (PPA). Thus, the light scattered by the Earth's atmosphere is governed by physics of the radiative transfer equation (RTE) with proper boundary conditions in the SSA system. In satellite and aircraft remote sensing, however, the PPA model is usually assumed to compute the lookup tables and convert the sensor-measured signals to the desired physical and optical quantities.

The PPA assumption is a simple yet very good approximation for solar and sensor zenith angles < ~ 80°. Note that the solar and sensor zenith angles here are defined as a measure at the local surface. In the PPA assumption, however, the solar zenith angles ≥90° is not defined. When the solar zenith angles ≥90° in the PPA system; i.e., when the Sun is below the horizon, there will be no light scattered out to the top of the atmosphere (TOA) or at the bottom of the surface. We would experience complete darkness in this situation.

The ocean color satellite sensor Sea-viewing Wide Field-of-view Sensor (SeaWiFS) [*Hooker et al.*, 1992] acquired imageries with the solar zenith angles ≥90° and provided good examples of the Earth's curvature effects on the light-scattering processing in the SSA system.

By Menghua Wang

This phenomenon is described and discussed in this article.

The SeaWiFS Measurements

The primary goals of SeaWiFS, which was successfully launched on 1 August 1997, are routine global ocean color measurements and ocean bio-optical property product generation. In its more than 5 years of operation, SeaWiFS has been continuously providing high-quality ocean color products [*McClain et al.*, 2003]. SeaWiFS has 8 spectral bands centered at 412, 443, 490, 510, 555, 670, 765, and 865 nm, with bandwidth of 20 nm for the 6 visible bands, and 40 nm for the 2 near-infrared (NIR) bands. The NIR bands are used for the purpose of the atmospheric correction [*Gordon and Wang*, 1994], which is to remove the atmospheric and surface effects and derive the visible signals exiting from the ocean waters. On 26 June 2000, SeaWiFS acquired imageries with significantly extended coverage, adding about another 5 minutes to the normal 40-minute recording duty cycle. This was a test for the SeaWiFS coverage capability and to find a proper additional coverage for the SeaWiFS routine operation.

For the test purpose, the SeaWiFS coverage for that specific orbit was extended significantly. Figure 1(a) provides the SeaWiFS global orbit coverage for 26 June 2000. It shows the southern extended coverage for a particular orbit (comparing with other normal orbits) covering part of the continent of South America.

Figure 1(b) shows the corresponding SeaWiFS-measured radiance image (RGB) for the part of the southern extended coverage, which is located around 60°S latitude and 62°W longitude. To clearly demonstrate the differences, the brightness of the image Figure 1(b) has been slightly enhanced. For the dashed line in Figure 1(b), the SeaWiFS-measured radiances (normalized to the extra-terrestrial solar irradiance) were plotted as a function of the solar-zenith angle for the spectral bands of 443, 510, and 670 nm (Figure 1(c)). The solar-zenith angle for the dashed line varies from ~76° to ~94° (from the top to the bottom of the line), the sensor-zenith angle is ~28°, and the relative azimuth angle is ~42°.

It is obvious that, although the values are relatively small, the TOA radiances are still significant for the solar zenith angles ≥90°. It is also interesting to note that, for the larger solar zenith angles, the normalized radiance contribution at the red bands becomes more important. It exceeds the radiance contributions at the blue and green bands for solar zenith angles ≥90°. In these cases, the SeaWiFS-measured imagery looks more or less reddish as shown in Figure 1(b).

The Model Simulations and Comparisons

To understand and interpolate the SeaWiFS measurements, the various radiative transfer simulations for the SSA model were carried out using the backward Monte-Carlo method that was developed by *Ding and Gordon* [1994]. The radiative transfer code is for the SSA model bounded by a Fresnel reflecting ocean surface, and has been slightly modified for cases with atmospheres composed of any type of scattering particles; e.g., water clouds. In addition, the code has been modified to use inputs of the solar-sensor geometry defined at the PPA system (at the local surface).

Figure 2 shows the comparisons of simulated results with the SeaWiFS measurements at

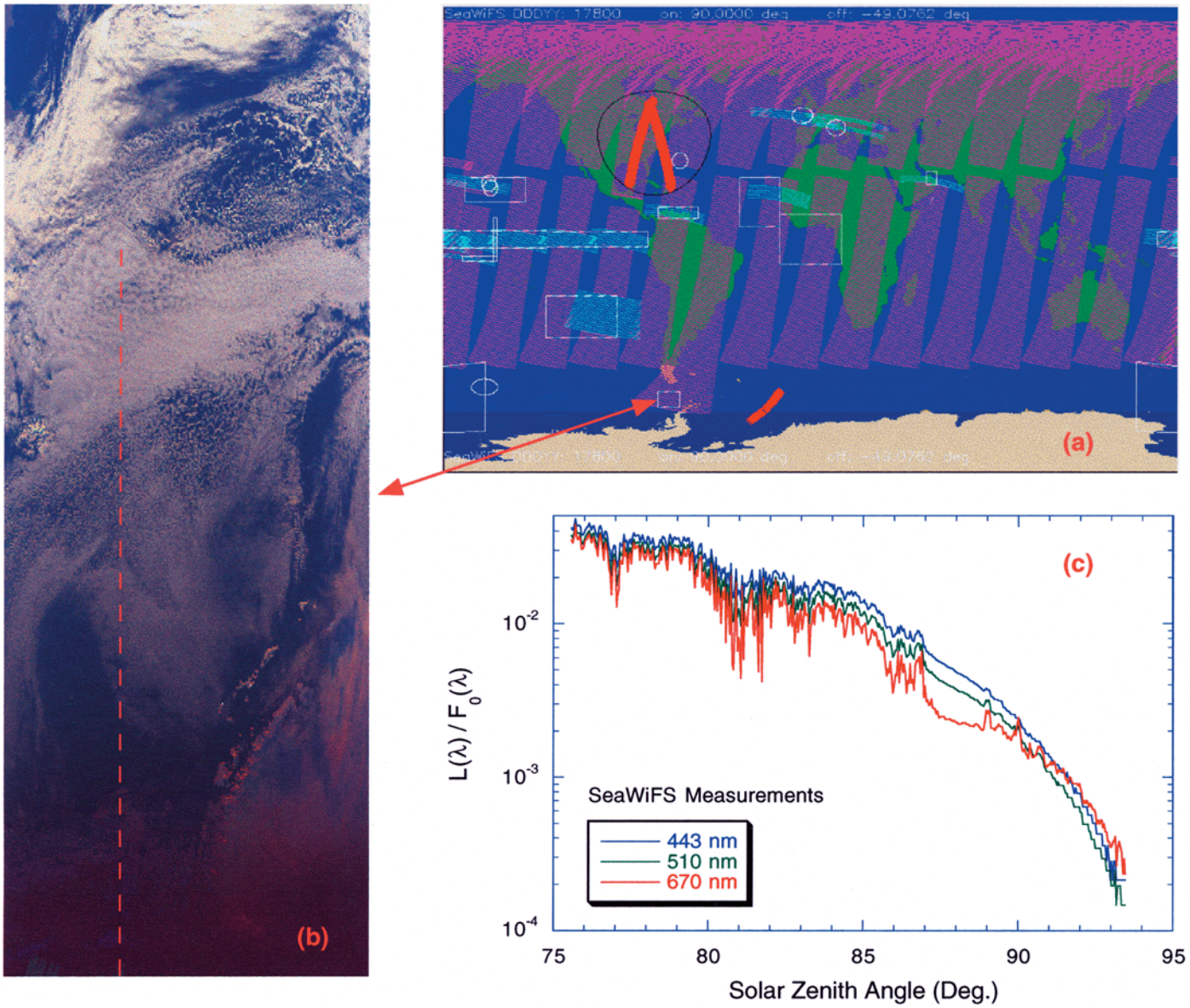

Fig. 1. The extended coverage acquired by SeaWiFS on 26 June 2000 at location around 60°S latitude and 62° W longitude for (a) the image of the global orbital coverage, (b) the SeaWiFS-acquired RGB radiance image, and (c) the SeaWiFS-measured radiances (443, 510, and 670 nm) as a function of the solar zenith angle for the dashed line in the panel (b).

wavelengths 443 and 670 nm for atmosphere composed of the molecules (Rayleigh scattering), molecules and aerosols, and molecules and water clouds. In Figure 2, the SSA simulations were carried out for the sensor located at the altitude of 705 km (SeaWiFS orbit) with the various SSA atmospheres. Detailed descriptions of the solar-sensor geometry in the SSA model can be found in *Ding and Gordon* [1994].

For each Monte-Carlo simulation, ten million photons were used. Figures 2(a) and 2(b) are comparison results for an atmosphere composed of molecules (Rayleigh scattering) with various physical thickness of the atmospheric layer (from 10 km to 100 km). Results from the plane-parallel atmosphere (indicated as "ppa") are also provided for comparisons. Clearly, PPA model makes significant errors (underestimation) for the solar zenith angles > ~85°. Figures 2(c) and 2(d) show comparison results for a two-layer SSA model with aerosols located at the bottom 2-km layer (mixed with 22% of molecules). The *Shettle and Fenn* [1979] maritime aerosol model with relative humidity of 80% (M80) and aerosol optical thickness at 865 nm of 0.1 were used in these simulations.

Figures 2(e) and 2(f) demonstrate a comparison of results for a two-layer SSA model with water clouds located at the bottom 2-km layer (mixed with 22% of molecules). These are simulations for the cloud optical thickness τ_c of 8 and an effective particle radius r_e of 8 μm with the various physical thicknesses of the SSA layer; e.g., symbol "20, 2 km" is the result for a two-layer SSA atmosphere with total physical thickness of 20 km and a 2-km layer at the bottom. Signals contributed from ocean waters are ignored in all these simulations. They are negligible in these cases.

As shown in Figures 1 and 2, the TOA radiances at the top part of the dash line (solar zenith angles from ~76° to ~85°) can be best simulated with cloud optical thickness ~8, while the bottom part of the dashed line can be well-approximated with the M80 model for aerosol optical thickness of 0.1. These are comparisons in qualitatively. It is interesting to note that, however, for the very large solar zenith angles (> ~85°), the TOA radiance is very sensitive to the physical thickness of the atmospheric layer assumed in the simulation. Indeed, for the very large solar zenith angles, the TOA radiance is much more sensitive to the change of physical thickness of the layer than to the optical properties of the medium (e.g., compare results of Figures 2(c) and 2(e)). This is because, for the SSA model with the large solar zenith angles, photons that are exiting to the TOA through scattering process are limited by the solar-sensor geometry and physical thickness of the layer. The thicker the layer is, the larger the probability that photons can be scattered into the sensor viewing direction; hence, the larger the sensor-measured radiance.